Int. J. Electrochem. Sci., 15 **(2020)** 6645 – 6662, doi: 10.20964/2020.07.11

International Journal of
ELECTROCHEMICAL
SCIENCE
www.electrochemsci.org

Synthesis and Characterization of ZnO /4, 5-imidazoledicarboxylic acid Composite and Its Application for Hemoglobin Determination

Fang Wang, Shu Xian Zhao, Han Zeng[*]*, Wen Shan Huo*

Chemistry and Chemical Engineering Academy, XinJiang Normal University, Urumuqi 830054, XinJiang Uyghur autonomous region, People's Republic of China
[*]E-mail: zenghan1289@163.com

Received: 23 February 2020 / *Accepted:* 13 April 2020 / *Published:* 10 June 2020

Petaloid-shaped ZnO grafted with 4,5-imidazoledicarboxylic acid was proposed as a composite to entrap Hemoglobin molecules through the synergistic effect of covalent bonding and adjacent complexation between the hetero-atoms of the imidazolyl ring and the heme sites in Hemoglobin. The morphology, structural features, and physiochemical properties of the composite with Hemoglobin anchoring were investigated by photography, spectroscopy, and electrochemical methods, as well as the mechanism of charge shuttle of the heme protein into the composite and the dynamics of enzymaticcatalysis. Experimental results revealed that intricate interactions between components of the complex and the integrated Hemoglobin molecules alter the mechanism of charge shuttle between cofactors in the enzyme and the conductive matrix with partial heme sites in coordination with the imidazolyl ring as an intra-molecular electron relay. Such interactions are also responsible for the process of substrate binding for the cofactors in the redox protein. The rapid kinetics of heterogeneous charge convection is found to be 89.0 s^{-1} with a unique pattern of two electrons per proton. This interactions would also lead to a lower affinity to hydrogen peroxide (893.0 μM), a high detection limit (0.9 mM), inferior sensitivity (4.5×10^{-5} A•L•mol^{-1}) and moderate kinetics of substrate attachment and transformation (1.9×10^{6} and 29.8 s^{-1}).

Keywords: petaloid ZnO, 4, 5-imidazoledicarboxylic acid, adjacent coordination, enzymatic electro-catalysis, Hemoglobin

1. INTRODUCTION

It is well-known that the dynamics of electron shuttle between cofactors within redox protein molecules and conductive supporters could determine the efficiency of enzymatic electro-catalysis. Many efforts [1-4] have been devoted to the achievement of direct electron transfer between redox proteins and enzyme carriers with favorable rates. Recent studies [5, 6] indicate that small scale

inorganic materials functionalized by aromatic or hetero-aromatic groups would facilitate the integration of direct electrochemistry of protein molecules Most reports [7, 8] focus on the catalytic performance of nanomaterial-based electrodes with protein anchorage and direct electrochemistry of enzyme-based electrodes.

Metal oxide semi-conductors have been applied in bio-analysis and bio-fuel cells for decades because of its unique features such as high surface area, facile preparation, low toxicity, and favorable chemical stability. Researchers claim that spherical ZnO with a hollow structure and ZnO composites, in combination with other nano-materials or small organic molecules as a matrix to accommodate bio-molecules [9-11], could achieve direct electron shuttle between the redox sites within bio-molecules and the conductive interfaces. However, the disadvantages of metal oxides as the fundamental units of bio-electrochemical devices rely on their high resistance for charge convection and undesirable rates of enzyme loading. It should be noted that the mechanism of charge shuttle and catalysis for the electrode on the basis of metal oxides with enzyme integration has not been discussed adequately so far [12-13].

Imidazole rings are a typical electron deficient aromatic ring featuring a non-centric symmetric structure. Strong electron-donating or electron-withdrawing groups could be grafted to the matrix of imidazole-like compounds and intra-molecular charge shuttle could be achieved within such systems [14-15]. Furthermore, interactions between hetero-atoms within imidazolyl units and redox centers in enzyme molecules (e.g. hydrogen bonding and adjacent coordination) could impose a considerable influence to the direct electrochemistry of the incorporated redox proteins and enzymatic catalysis. Only a few studies have reported on this strategy[16]. The use of imidazolyl compounds as ligands and components of enzyme matrixs [6] could increase the enzyme capacity of carriers made of inorganic materials functionalized by hetero-aromatic groups. and would help to improve the energy output. Hemoglobin (Hb) is a classical type of heme protein with four cofactors which are embedded into the insulated backbone of the protein molecule. Many attempts [17-20] have been made to achieve direct electron transfer and fruitful catalysis for specific substrates of Hb incorporation into suitable supporters.

The objective of this article is to analyze the impact of the interactions between components of the enzyme matrix and the immobilized Hb on the intra-molecular charge transport within ZnO-imidazolyl composites with redox integration, and to elucidate the mechanism in the Hb-induced electrochemical reduction of hydrogen peroxide. ZnO covalently coupled with imidazolyl groups was proposed as a structure capable of accommodating Hb molecules. Hb-based electrodes were prepared based on ZnO-imidazolyl group composites with Hb linkage via drop-casting. Geometrical features and surface chemistry of the composite, configuration in Hb cofactors as well as the physiochemical properties of the composite with protein accommodation were characterized by multiple techniques including spectroscopy, electrochemistry and photography. The electrochemical behavior and electrocatalytic efficiency of Hb-based electrodes based on ZnO-imidazolyl composites were investigated and evaluated by electrochemical means. Quantitative analysis of Hb-involved catalysis of H_2O_2 electro-reduction not only would clarify the rate limiting step of the catalysis but could also promote a deeper understanding of important physiological activities such as respiration, nervous reflex, and stress reaction.

2. EXPERIMENTAL SECTION

2.1 Reagents and apparatus

Hb from bovine blood (Molecular weight: ~64500 g•mol^{-1}) and *N*-(3-Dimethylaminopropyl)-*N'*-ethylcarbodiimide hydrochloride (EDC) were provided by Sigma-Aldrich chemical reagent Co., Ltd, USA. *N*-hydroxysuccinimide (NHS) was purchased from Aladdin Reagent Co., Ltd, China. (3-Aminopropyl) triethoxysilane (APS) and 4, 5-imidazoledicarboxylic acid (H_3IDC) were purchased from Macklin biotech Co., Ltd, Shang-Hai in China. Chitosan (CTS, degree of deacetylation higher than 90 %, molecular mass: ~250000 g•mol^{-1}) as a film-forming reagent was obtained from Sinopharm Chemical Reagent Co., Ltd. (China). Other routine chemicals with analytical purity throughout the manuscript were purchased from Aladdin Reagent Co., Ltd, China or Sinopharm Co., Ltd (China). The electrolyte used in this manuscript was 0.2 M phosphate buffer (PBS) with modulated pH which was prepared following a previously published method [13]. Nitrogen gas with high purity was obtained from Kangdi Special Gas Co., Ltd, China.

The LG16-W desktop high-speed centrifuge used in the experiment was purchased from Jingli Centrifuge Co., Ltd, Beijing in China. A KQ2200DE type ultrasonic cleaning apparatus was provided by Kunshan Ultrasonic Instrument Co., Ltd, Kun-shan in China. A glassy carbon electrode (GCE, diameter: 4 mm) was proposed as the basal supporter, While a Ag/AgCl (saturated KCl) electrode acted as the reference electrode, with a potential of approximately 197 mV relative to the normal hydrogen electrode (NHE). These electrodes were bought from Aida HengSheng Co., Ltd, Tianjin in China. Scanning Electron Microscopy (SEM) measurements were conducted on a SU8010 type field emission equipment (Co., Ltd in Japan). FTIR measurements were performed in a TENSOR-27 type infrared spectrometer (KBr tablet) from BRUKER Co, Ltd (Germany). A U-2810 UV-vis spectrophotometer from Shimadzu Corporation in Japan was used for UV-vis analysis. The amount of Hb integrated into the composite was determined on a ICP-AES 7400 type inductively coupled plasma spectrometer from Thermo Scientific Corporation, USA. Measurements of fluorescent spectroscopy (FRS) were performed on a CaryEclipse model spectroflurometer provided by Varian Co., Ltd in USA. Circular Dichroism (CD) measurements were performed on a chirascan spectropolarimeter (Applied Photophysics Ltd, in UK). XRD experiments were performed on a BRUKER D2 model diffractometer purchased from BRUKER Co, Ltd (Germany). Electrochemical tests were conducted on a Zahner Zennium electrochemical platform and a CHI-660E electrochemical working station which were supplied by Kronach in Germany and Chen-Hua Co., Ltd in Shang-Hai of China, respectively.

2.2 Preparation of flower-like ZnO-based electrodes with Hb immobilization

The procedure for the preparation of flower-like ZnO and its amination were described elsewhere [21-22]. The synthesis of the amino surface-tailored ZnO was performed as follows: 30 mL ethanol was poured into an aqueous solution of 16.0 g•L^{-1} $Zn(CH_3COO)_2•2H_2O$ and 12.0 g•L^{-1} citric acid. The mixture was stirred for 6 h. NaOH solution was added to the mixed solution under

vigorous stirring for 30 min. The mixture of reactants was ultrasonically dispersed for 15 min and the dispersed system was then transferred into a Teflon-lined stainless steel autoclave to incubate at 120 ℃ for 24 h. After cooling down to room temperature, the solid crude product was rinsed with trio-distilled water and ethanol several times. The product was then dried at atmospheric pressure to obtain petaloid-shaped ZnO. The dried ZnO was dissolved in ethanol and APS was added into the system. The system underwent vigorous magnetic-stirring for 4 h. and was later centrifuged and washed with absolute ethanol several times to obtain APS-functionalized ZnO. Later, 0.2 g of APS-functionalized ZnO were ultrasonically dispersed in 5 mL of distilled water. 0.2 g of H_3IDC dissolved in 10 mL distilled water were incubated in a solution containing EDC and NHS to activate the carboxylic groups. The dispersed phase containing the aminated ZnO was added slowly into the solution with activated H_3IDC for adequate incubation. The solid substance was removed centrifugally from the system at a rotating rate of 8000 round•min^{-1}. The solution was later washed first with distilled water and then with ethanol. Finally, it was dried in air overnight. The as-prepared complex made of ZnO and H_3IDC was denoted as H_3IDC-ZnO. 12 mg of H_3IDC-ZnO were added to 3.0 mL of 0.2 M PBS with EDC *vs*. NHS with a molar ratio of 5:1 and the mixture was dispersed under magnetic stirring for 2 h. Subsequently, 3 mg of Hb were mixed with the discrete under moderate magnetic stirring for 1 h. The viscous mixture obtained was incubated in a refrigerator at 4 ℃ overnight to allow sufficient interaction between Hb and the protein carrier. The composite with Hb integration was designated as Hb/H_3IDC-ZnO. The loading amount of Hb integration into the composite was evaluated as 233.3 mg•g^{-1} by inductively coupled plasma atomic emission spectroscopy (ICP-AES) and its estimation was similar to a previously described method [13].

On the basis of composite with protein accommodation, an Hb-based electrode was prepared via drop-casting. 10 μL of fluid Hb/H_3IDC-ZnO was pipetted onto the surface of GCE which was pretreated as described elsewhere [16]. 2.0 μL of acetic acid solution with a CTS mass ration at 3% as a film-forming reagent was dripped onto the interface of the basal electrode over-coated by the complex with Hb accommodation. The electrode covered by the CTS thin film was dried in a buckled beaker to obtain the Hb-based electrode, which was named as Hb/H_3IDC-ZnO/GCE.

2.3 Direct electron transfer and catalytic effect on the reduction of hydrogen peroxide by Hb /H_3IDC-ZnO

The direct electrochemistry and catalytic function on the electrochemical reduction of hydrogen peroxide by the Hb-based electrode were investigated and evaluated by a variety of electrochemical methods including CV, differential pulse voltammetry (DPV), and chronoamperometry (CA). These measurements and tests were carried out on a Zahner Zennium electrochemical apparatus and a CHI-660E electrochemical analyzer. All experiments were performed at the local pressure of 94.6 kPa and normal temperature of 25.2+0.4 ℃. The potentials described throughout this manuscript were relative to the NHE. The active area was determined as the slope of the redox peak current square-root of scanning rate linear-fitting plot for testing electrode in solution with $K_3Fe(CN)_6$/$K_4Fe(CN)_6$+KCl as electrochemical probing species as described elsewhere [23]. Aliquots of 50.0 mM of PBS with H_2O_2 were pipetted into a blank solution

to obtain electrolytes with variable substrate concebtrations during the acquisition of the CA curves. for H_3IDC-ZnO complex-based electrode with Hb immobilization. The applied potential of the CA experiment was set at the onset potential of the limiting catalytic current as suggested earlier [24]. The operational parameters of DPV were as follows: potential sweeping ranging from -1.0 to 1.0 V, step width at 0.05 s, and step height at 5 mV.

3. RESULTS AND DISCUSSION

3.1 Characterization of composite with enzyme tethering

SEM images of ZnO (A), ZnO surface-tailored by H_3IDC (B) and H_3IDC-ZnO complex with Hb accommodation (C) are shown in Fig.1. The morphology of H_3IDC-ZnO can be distinguished from that of ZnO by the partial disappearance of the inherent petaloid structure of the as-prepared ZnO (see enlargement in Fig.1A inset). Furthermore, the appearance of an irregular agglomeration on the surface of the complex can be observed in Fig.1B, which can be attributed to the bonding between the amino groups on the interface of the aminated ZnO and the carboxyl groups of H_3IDC, which leads to a random covalent linkage of the H_3IDC with the petaloid ZnO. The geometry of the ZnO-H_3IDC composite with Hb immobilization was different from cases described previously, due to the disappearance of the original flower-like structure of ZnO or H_3IDC-ZnO complex, and the relatively smooth surface of the complex with protein immobilization can be identified in Fig.1C. This suggests that the enzyme molecules could be anchored on the surface of the composite. Similarly, the coverage of Hb on the surface of the complex can be ascribed to the sophisticated interactions between the composite and the incorporated protein molecules [25]. These interactions are comprised of the random coupling of the enzyme molecules with the complex through the formation of amido bonds and adjacent ligation as demonstrated previously [26].

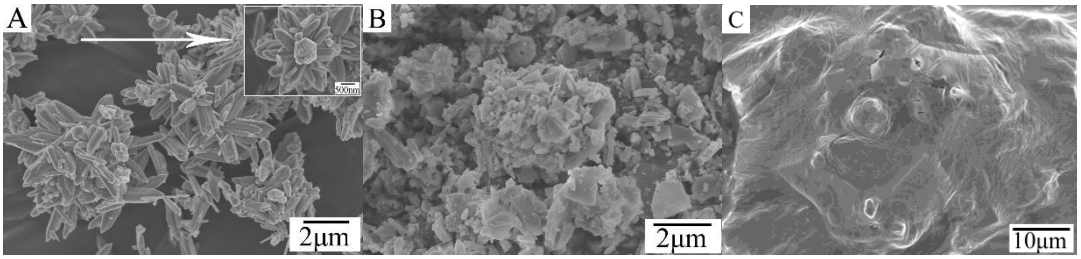

Figure 1. SEM images of petaloid ZnO(A), ZnO surface-grafted by H_3IDC(B) and composite of ZnO-H_3IDC with Hb immobilization (C)

Fig.2 shows the FTIR spectra of H_3IDC, H_3IDC-ZnO complex, free Hb, and composite with Hb anchoring. It can be noticed that the FTIR spectra of ZnO and ZnO functionalized with the amino group were included in the inset graph of Fig.2. The sharp absorption band at ~422.0 cm^{-1} and the relatively weak absorption bands at 3357 and 1568 cm^{-1} can be ascribed to the stretching vibrations

of Zn-O in ZnO, and the stretching vibrations and bending vibrations of -OH on the surface of ZnO, respectively [22, 27]. Three moderate absorption peaks at 1609.4, 1687.2 and 1531.4 cm^{-1} could be recognized in the spectrum of H_3IDC and the appearance of these peaks indicates the existence of C=N in the imidazole unit, C=O (within carboxyl group in connection to imidazole matrix) and C=C (within imidazole ring), respectively. A wide and broad absorption band at ~3427.3 cm^{-1} confirmed the accomplishment in the modification of ZnO with amino groups. Both diagnostic peaks at 1755.1 and 3209.4 cm^{-1} in the spectrum of the H_3IDC-ZnO composite corroborated the presence of the amido bond, and the absorption band at ~445.1 cm^{-1} of Zn-O demonstrated the successful linkage of H_3IDC to ZnO via covalent coupling. It should be noticed that most absorption peaks in the spectrum of the composite with Hb integration were similar to those in the spectra of free Hb and the H_3IDC-ZnO complex. An absorption band at 1649.0 cm^{-1} could be observed in the spectra of free Hb and composite with Hb incorporation. This characteristic peak should be attributed to the amido I absorption band in free Hb and it can be observed that the original structure of this site in the heme protein was substantially intact. However,a different featuring band for free Hb and complex with Hb coupling showed observable differences. This suggests that an apparent violet shift of the amido II band for the composite with entrapped protein in comparison to that for free Hb (strong absorption bands at 1564.2 and 1537.0 cm^{-1}) could be identified in Fig.2. Consequently, the intricate interactions between the complex and the integrated enzyme molecule (e.g. adjacent ligation between the composite and the Hb molecule as reported earlier [16]) would contribute to such shift to high wave-numbers.

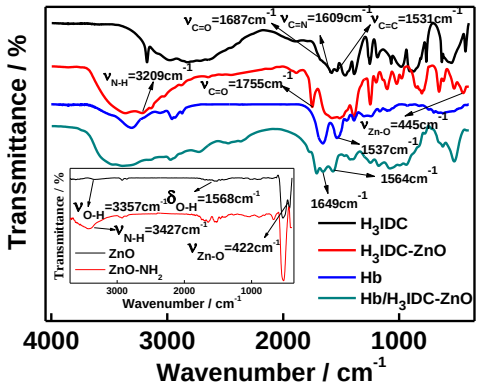

Figure 2. FTIR spectra of H_3IDC, composite of ZnO-H_3IDC, free Hb and complex with protein accommodation, inset graph: ZnO and aminated ZnO

The UV-vis spectra of the petaloid-shaped ZnO, H_3IDC, H_3IDC-ZnO composite, free Hb, and H_3IDC-ZnO complex with tethered Hb are exhibited in Fig.3. It can be seen from Fig.3 that a common absorption band at ~255.3 nm can be discerned for the three cases: H_3IDC, H_3IDC-ZnO complex, and the complex with enzyme accommodation. This band should be considered as the typicalл→л* electron transition within the imidazole ring. Two strong and sharp absorption peaks at 212.5 and 405.4 nm as well as a weak one at 277.1 nm could be discriminated in the spectrum of free Hb. The former two bands should be ascribed to n→л* electron transitions within the peptide chain

of the heme protein and the featuring peak of the porphyrin ring [28], respectively. The latter one could be described as the classic л→л* electron transition within the aromatic ring of the amino acid (such as tyrosine and tryptophane). Furthermore, a common band at ~220.1 nm for the four systems can be observed and should be attributed to a typical absorption band of charge transfer [29]. Interestingly, a degree of red-shift at ~260.1 nm for the л→л* electron transition in the spectrum of the H_3IDC-ZnO complex with Hb integration can be observed, compared to that of the composite alone. This red-shift can be attributed to the enlargement of the conjugation system via the introduction of the porphyrin ring in the Hb into the H_3IDC-ZnO complex. The extinction of the peak at 212.5 nm attributed to the free protein in the spectrum of the composite after enzyme incorporation can be identified in Fig.3. This confirm the presence of complicated interactions between the enzyme carrier and the immobilized protein molecules. Such interactions include the abutting ligation between Zn^{2+} within the complex and hetero-atoms in the surface of H_3IDC, as well as neighboring coordination between the $Fe^{2+/3+}$ ions in the heme cofactor and the hetero-atoms within the imidazole ring of the complex. It should be noticed that an inherent soret band at 405.4 nm in the spectrum of the composite with enzyme tethering was kept intact even in the presence of the sophisticated interactions depicted previously. This implies that the original configuration of the heme site in Hb was retained [30-31], and that the H_3IDC-ZnO composite could provide a preferred micro-environment to maintain the intrinsic bio-activity of the free Hb after its integration into the complex.

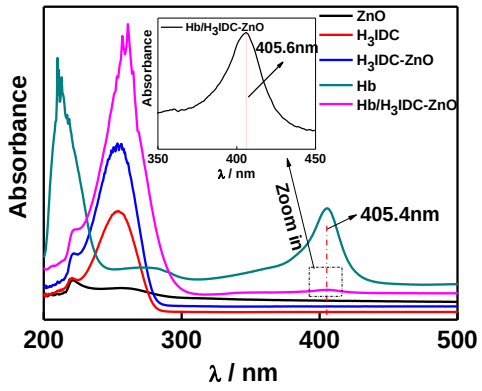

Figure 3. UV-vis spectra of ZnO, H_3IDC, ZnO surface-modified by H_3IDC, free Hb and composite with Hb immobilization

Fig.4 shows the XRD spectra of ZnO, H_3IDC, and H_3IDC-ZnO powder. It can be observed that the nine featuring peaks in the ZnO spectrum were consistent with those in the standard diffraction card JCPDS (No.79-0207). This suggests that petaloid-shaped ZnO with a relatively high crystallinity was successfully prepared. Moreover, featuring peaks H_3IDC and ZnO could be discerned from the spectrum of the composite, demonstrating that H_3IDC was covalently coupled to the interface of ZnO. The decreased intensity of similar diffraction peaks in the spectrum of the composite suggested decreased crystallinity and augmented dimension [32], which is in accordance

with previous analysis.

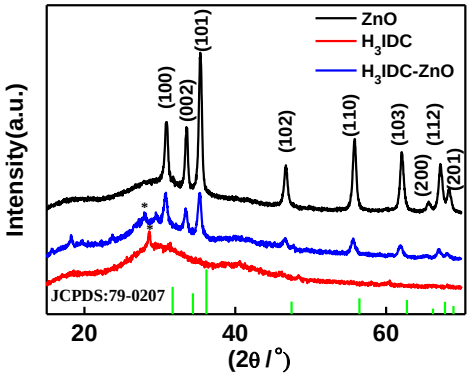

Figure 4. XRD patterns of petaloid ZnO, H_3IDC and H_3IDC-ZnO powder

The CD spectra of PBS with Hb with a density of 0.5 g•L^{-1}, a dispersed phase of H_3IDC-ZnO, and the H_3IDC-ZnO complex with Hb entrapment are illustrated in Fig.5. Two negative absorption bands at 209 and 221 nm in the spectrum of free Hb can be identified in Fig.5. Both peaks should be ascribed to л→л* and n→л* electron transitions of α-helix for the peptide within the heme protein molecule. No distinct negative band could be observed within the scanning range of the wavelength in the spectrum of H_3IDC-ZnO. On the other hand, H_3IDC-ZnO with Hb linkage could be distinguished from the previous systems, due to the disappearance of the negative absorption band at 221 nm and a shift of the band at 209 to 201 nm after Hb integration into the H_3IDC-ZnO composite. Moreover, the strength of the latter one in the spectrum of the complex with Hb coupling was attenuated substantially, which implies that the H-bond meshwork was disrupted from the combination of Hb with the complex via chemical bonding and adjoining complexation [33]. Another consequence of Hb coupling into complex was the reduction in the content of the α-helix, which suggests improved hydrophilicity.

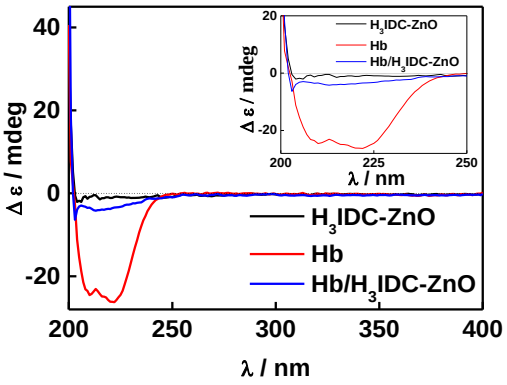

Figure 5. CD spectra of free Hb, H_3IDC-ZnO composite and complex with Hb anchoring

Fig.6 depicts the emission fluorescence spectra of the mixed system with different H_3IDC:Hb ratios. The inset graph A represents the Stern-Volmer calibration curve for the interaction between Hb and H_3IDC, and the inset graph B represents the linearly-fitted plot of lg[(F_0-F)/F] versus lg C_Q. A series of broad and intense fluorescence emission bands in the range of 335 to 350 nm can be discerned from Fig.6. These emission peaks originated from residues of tyrosine and tryptophane [34]. The intensity of these bands decreases with increasing H_3IDC content in the mixed system and the location of these emission peaks red-shifted. An attenuation in the intensity of the emission peak for Hb in combination with H_3IDC as well as a red-shift in the emission band of Hb coupled to H_3IDC can be attributed to the alteration of the configuration of Hb, originated from the complicated interactions between the enzyme molecule and H_3IDC. Such interactions would lead to the exposure of tyrosine and tryptophane in the secondary structure and would result in the increased polarity of the micro-environment for the amino acid residues [35]. The fluorescence quenching constant (K_q) was calculated to be 3.04×10^{10} L•(mol•s)$^{-1}$ from data analysis as described previously [36]. This value was slightly higher than the thereshold of K_q for bio-macromolecules for most quenching reagents (2.0×10^{10} L•(mol•s)$^{-1}$), which indicated that the extinction model of fluorescence should be classified as static quenching. Additionally, it suggests that the combination of Hb with H_3IDC would result in the formation of a composite without fluorescence emission. The number of binding sites and combination coefficient could be estimated as 1.0 and 4.78×10^2 L•mol^{-1} according to the same method described elsewhere [36]. This result implies that the heme site of Hb in coordination with H_3IDC is carried through at a molar ratio of 1:1, also revealing that the strength of the combination was not enough to distort the inherent configuration of the cofactors in Hb. This suggests that the heme site in the protein molecule still possess its innate catalytic activity, and a distinct charge transfer mechanism for Hb in combination with complex could be analyzed.

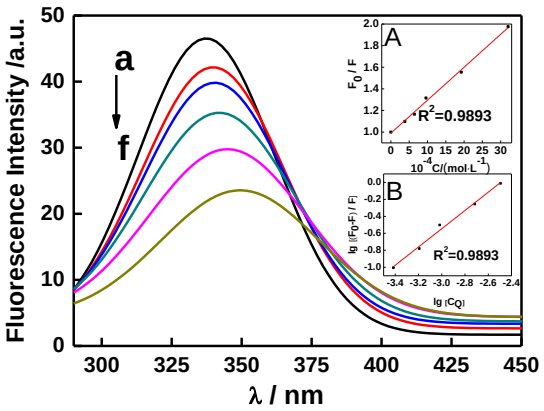

Figure 6. FRS spectra of mixing solution with constant content of Hb (0.25 mg•mL^{-1}) and modulated consistencies of H_3IDC (a-f indicating concentrations of H_3IDC: 0, 0.06, 0.10, 0.15, 0.30 and 0.50 mg•mL^{-1}), inset graph A is Stern-Volmer plot for interaction of Hb and fluorescence quenching reagent; inset graph B is Linear-fitting plot of lg[(F_0-F)/F] versus lg C_Q

EIS spectra and CVs of the bare GCE, the electrode over-coated by petaloid-shaped ZnO,

GCE covered with the H_3IDC-ZnO composite and the electrode of H_3IDC-ZnO complex with Hb are illustrated in Fig.7A and Fig.7B. The impedance of the GCE over-coated by ZnO was much higher than that of the bare GCE due to the introduction of the classical P-type semiconductor with a wide band gap. An apparent decrease in the resistance of the charge shuttle could be discerned compared to the electrode modified by the H_3IDC-ZnO complex, likely due to the introduction of electro-active sites within the composite and an alteration in the electronic structure of the hetero-ring. The latter originated from the adulteration of hetero-atoms in the conjugation system [15]. The existence of electro-active groups within the composite would favor the electron transfer of electrochemical probing species to some extent. Results of CV for those electrodes coincided with the analysis of the EIS spectra. The GCE modified by the H_3IDC-ZnO composite with Hb coupling could be distinguished from the other systems due to an increased impedance and the disappearance of the redox band of $K_3Fe(CN)_6/K_4Fe(CN)_6$. This change was likely due to the interaction between $Fe(CN)_6^{3-}/Fe(CN)_6^{4-}$ and the incorporated Hb molecules. This suggests that the complexation of $Fe(CN)_6^{3-}/Fe(CN)_6^{4-}$ with residual amino acid on the surface of Hb would hinder the redox process between the electrochemical probing species and the conductive matrix. This deduction was consolidated by the FRS of the mixed solution with constant Hb content and variable quenching reagent concentration (i.e. $Fe(CN)_6^{3-}/Fe(CN)_6^{4-}$), which demonstrates that the combination of Hb with $Fe(CN)_6^{3-}/Fe(CN)_6^{4-}$ would engender a complex without fluorescence emission.

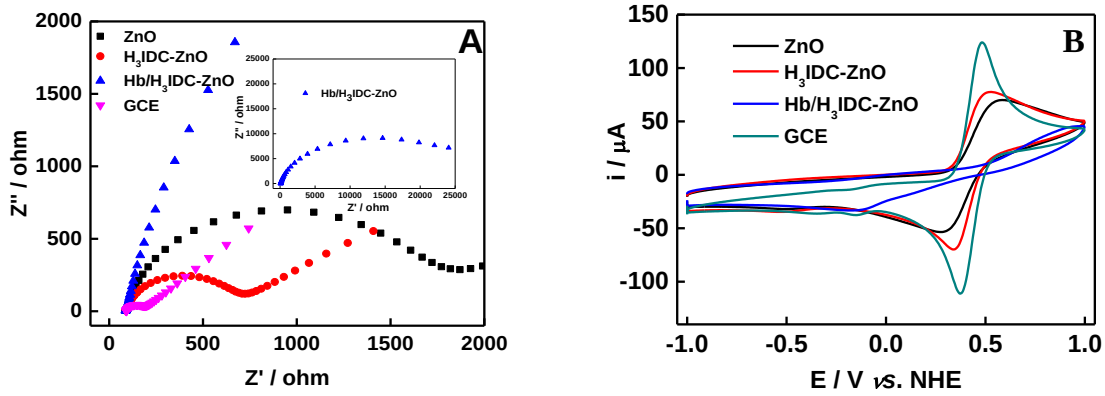

Figure 7. EIS spectra(A) and CV curves(B) of supporting electrode, GCE capped by ZnO, basal electrode over-coated by H_3IDC-ZnO composite and GCE modified by complex with Hb integration in electrolyte of 2.5 mmol•L^{-1} $K_3Fe(CN)_6$+2.5 mmol•L^{-1} $K_4Fe(CN)_6$+0.1mol•L^{-1} KCl, scanning rate at 100 mV•s^{-1}

3.2 Electrochemical features and catalytic performance on the electro-reduction of hydrogen peroxide for the GCE based on H_3IDC-ZnO composite with Hb integration

CVs of GCEs over-coated by ZnO, H_3IDC-ZnO complex, and composite thin film with Hb entrapment in de-aerated PBS (pH=7.0) are exhibited in Fig.8. Only one broad and weak oxidation peak at ~330 mV could be discriminated from the CVs of GCE capped by the petaloid-shaped ZnO and the GCE over-coated with H_3IDC-ZnO. The enhancement of the oxidation peak could be attributed to the process of intra-molecular charge transfer within the imidazole ring [29]. A pair of

asymmetric peaks at a potential of ~-115 mV could be observed in the CV of Hb/H_3IDC-ZnO/GCE. This quasi-reversible electrochemical signal should be ascribed to a unique feature for the heme site of Hb in the status of adjacent coordination. Competitive interactions between hetero-atoms in the imidazole ring and metal ions within the complex (Zn^{2+}) or the protein molecule (Fe^{2+}/Fe^{3+}) would impose a considerable influence on the mechanism of intra-molecular electron convection. This means that the electrochemical reaction of the heme site in Hb was distinct from previously described ones [31] and this redox site would be more oxidative. The impact of competitive ligation on the electron transfer was similar to that of enzyme-induced electro-reduction of di-oxygen molecules in the presence of an electron mediator [37]. In another words, the heme site in complexation with H_3IDC could act as an intra-molecular electron relay. Furthermore, the coverage of electrically-wired Hb molecules was calculated as 1.78×10^{-11} mol•cm^{-2} from the normalization of the mean integration area of the redox peaks to the product of potential sweeping rate, the numbers of electron shuttle in the process of electrochemical reaction, the active area of the electrode and the Faraday constant, according to a previous publication [38]. Moreover, another weak reduction peak at ~-0.72 V could be discerned from Fig.8. This electrochemical signal is usually assigned to the electro-reduction of oxygen attachment on the enzyme matrix via physical adsorption or chelation [16]. Di-oxygen molecules entrapment in the H_3IDC-ZnO composite was validated with Clark oxygen electrodes as demonstrated previously [39].

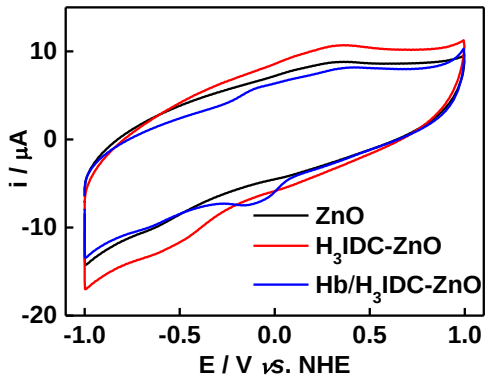

Figure 8. CVs of GCE modified by ZnO, supporting electrode over-coated by H_3IDC-ZnO composite and basal electrode capped by thin film of complex with Hb integration in deaerated PBS (pH=7.0), sweeping rate: 200 mV•s^{-1}

Fig.9 and its inset shows the CVs of the static electrode on the basis of the composite with Hb incorporation in N_2-purged PBS recorded at a variable potential-sweeping rate as well as the dependence plots of anodic/cathodic current. It is evident from Fig.9 and its inset that the oxidation/reduction current peak would augment linearly with increasing potential sweeping rate. The gap between the anodic and cathodic potential peak is proportional to the increase in the potential scanning rate. It should be noticed that the potentials of the oxidation peaks are almost invariable at different sweeping rates while the reduction ones show a negative shift with increasing sweeping rates. The ratio of the anodic to cathodic current peak increased from 0.5 to 0.9 with increasing sweeping rate. An improvement in the reversibility of charge transfer indicated that the

existence of H_3IDC as a redox group and a competitive ligand positively influence the dynamics of direct electron shuttle for immobilized Hb molecules. These fingings were different from a similar case described previously [30-31], in which the peak potential difference is almost identical under variable sweeping rates and the ratio of the anodic/cathodic peak current was close to 1 under different sweeping rates. This indicates that the redox process of Hb/H_3IDC-ZnO/GCE could not be simply classified into the typical surface-confined type or diffusion-controlled, but rather to an intermediate model or so-called mixed model of surface confining reaction and swaying process of electron shuttle. This conclusion was confirmed by the result of DPV experiments registered at variable pulse heights for the Hb-based electrode in N_2-purged PBS, as shown in Fig.10 A and B. The oxidation band at higher potentials in the positive scanning in relation to the electrochemical reaction of H_3IDC would decrease with increasing pulse height. This result implied that the kinetics of the heme sites within Hb in the presence of intricate interactions was superior to that of the redox group within the H_3IDC-ZnO composite.

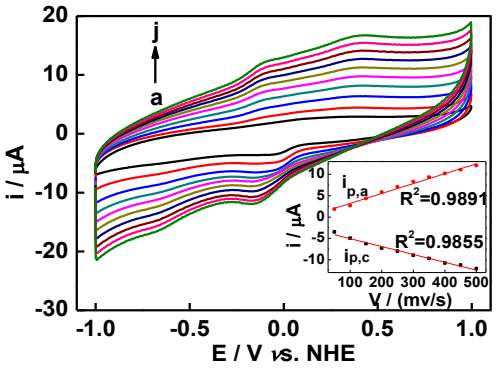

Figure 9. CVs of Hb/H_3IDC-ZnO/GCE in oxygen-free PBS (pH=7.0) recorded at variable scanning rates, curve a-j indicating scanning rate: 50, 100, 150, 200, 250, 300, 350, 400, 450, 500 mV•s^{-1}, inset graph: linear-fitting plots of anodic/cathodic peak current versus sweeping rate

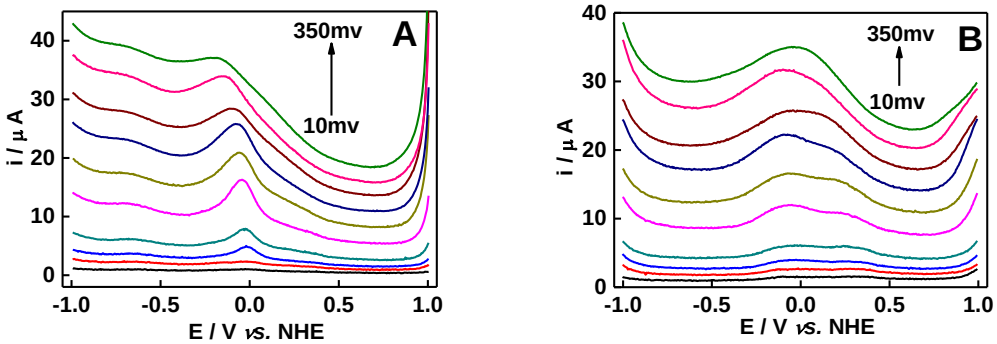

Figure 10. DPV curves of Hb/H_3IDC-ZnO/GCE in nitrogen-bubbling PBS (pH=7.0) registered at 200 mV•s^{-1} and variable pulse heights (from bottom to top: 10, 20, 30, 50, 100, 150, 200, 250, 300 and 350 mV) in the negative (A) and positive (B) potential sweeping

A pair of prominent redox peaks at ~-110 mV could be recognized and its electrochemical

reversibility increases at higher pulse height. These results confirm that two consecutive steps of electron transfer were included in the whole electrochemical reaction of the Hb-based electrode. Furthermore, a reduction band at~-0.7 V could be identified as reported previously and it was attributed to the electrochemical reduction of the attached di-oxygen molecules with high active energy.

A linearly-fitted plot of the difference between both peaks as a function of the logarithm of the scanning rate is displayed in Fig.11. The apparent rate constant of heterogeneous electron transferring (k_s) and charge shuttle coefficient (α) were calculated as 89.0 s^{-1} and 0.27. These dynamic parameters were calculated according to a previous report [40]. The value of k_s for the heme site within Hb in the status of adjacent coordination was much higher than that of the immobilized Hb in the absence of a similar ligation with abutting ligand (13.34 and 1.8 s^{-1}) [16, 40]. The favorable efficiency of electron convection confirmed the presence of sophisticated interactions, including adjacent complexation, which would promote the process of electron conveyance between cofactors in Hb and conductive matrix.

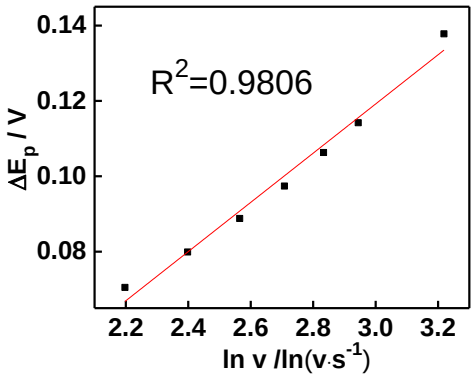

Figure 11. Linear-fitting plot of potential difference between oxidation peak and reduction one versus logarithm of potential scanning rate for Hb/H_3IDC-ZnO/GCE in quiescent nitrogen bubbling PBS

The CV plots of the complex-based electrode with Hb immobilization in a series of PBS with pH modulation are shown in Fig.12. Irregularity in the variation of the anodic/cathodic peak current ratio with increasing pH can be identified from Fig.12, which is likely due to perplexing interactions between the protein and elements of the composite. The cathodic peak potential for the Hb-based electrode would shift negatively with increasing pH of the PBS solution. The inset of Fig.12 displays the linear relationship between the potential peak reduction for the Hb-based electrode and the pH value of the electrolyte. The extrapolated slope of the linear plot was estimated to be -26.5 mV/pH, which suggests that the reduction process of the heme site in coordination with H_3IDC should be considered as a typical electrochemical reaction with one H^+ and two electrons involved. However, this conclusion was different from the observations made for the Hb-based electrodes described previously, in which one electron and one proton were involved for the case of heme proteins incorporated into agarose hydrogel and Hb entrapment in multi-wall carbon nano-tubes overlapped by ZnO coat [41]. This suggests that the unique feature of electrochemical reaction could originate

from the prominent change in the electron shuttle with additional oxidation of the electro-active group in H_3IDC-ZnO. Moreover, the catalytic current changed as a function of the pH of the buffer solution in the same way that the catalytic efficiency varied according to the pH value of the electrolyte for free the heme protein molecules. The curve presented a bell-like shape for the catalytic efficiency as a function of pH and the optimal pH was determined as ~6.8 [42] (data not shown). This result confirmed the previous deduction that the aboriginal activity of catalysis for free Hb could be maintained to a great extent after protein integration into the composite.

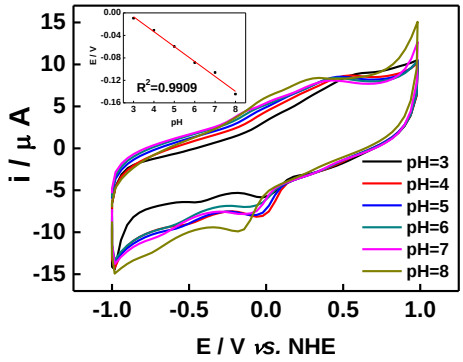

Figure 12. CV curves of basal electrode over-coated by thin film of H_3IDC-ZnO composite with Hb integration in electrolyte with controllable pH values, scanning rate: 200 mV•s^{-1}; inset graph: dependence of reduction peak potential on pH of PBS

The CVs of Hb/H_3IDC-ZnO/GCE in de-aerated electrolyte with varying concentration of H_2O_2, and the CA curve of the Hb-based electrode when stirring PBS with successive additions of substrate registered at a constant potential were obtained and are shown in Fig.13 A and B. The inset graph of Fig.13B provides the linear-fitted plot of the steady catalytic current versus the substrate concentration. In Fig.13A, a minor change in the strength of the oxidation peak and a gradual increase in the reduction current can be observed. These observations were in accordance with the typical feature of electrocatalytic reaction as demonstrated previously [43]. The onset potential of substrate electro-reduction was determined as ~25 mV vs. NHE. A desirable linear relationship between the steady catalytic current and substrate content could be maintained within the range of the testing sample. The sensitivity of this Hb-based electrochemical sensor and its detection limit were calculated as 4.5×10^{-5} A•L•mol^{-1} and 0.9 mM, respectively, from the inset graph of Fig.13B. The inferior sensitivity and higher detection limit compared with other similar systems with heme protein immobilization [41] indicated that complicated interactions between elements of the enzyme carrier and the immobilized protein could egenerate a negative impact on the performance of the as-prepared Hb-based electrochemical sensor. The rate constant of substrate binding (k_{sb}) and Michaelis constant (K_M) could be estimated to be 1.9×10^6 s^{-1} and 893.0 μM, respectively, derived from the Lineweaver-Burk plot. A moderate affinity to the substrate and mean kinetics compared to other similar cases (see Table 1) suggest that the interference from the intricate interactions between Hb and components of the composite in the chemical binding of hydrogen peroxide onto cofactors in Hb cannot be neglected. The turn-over frequency of the substrate from the normalization of the limiting catalytic reduction current of enzyme-induced hydrogen peroxide to coverage of electrical-wired

enzyme molecules was derived from extrapolation of linear reciprocal plot of the catalytic current versus substrate content in compliance with a same method demonstrated previously [44]. The value was calculated as 29.8 s^{-1}. Considering the moderate apparent diffusion coefficient for substrate-H_2O_2being 1.2×10^{-5} $cm^2 \cdot s^{-1}$ [45], an inferior mass transfer rate constant was calculated as 6.7×10^{-5} s^{-1} from the normalization of the diffusion coefficient by the active surface area of the composite-based electrode. On the basis of quantitative analysis on the dynamics of the procedures involved in the enzyme-induced catalysis, substrate diffusion could be determined as the rate limiting step of the whole electro-catalysis process.

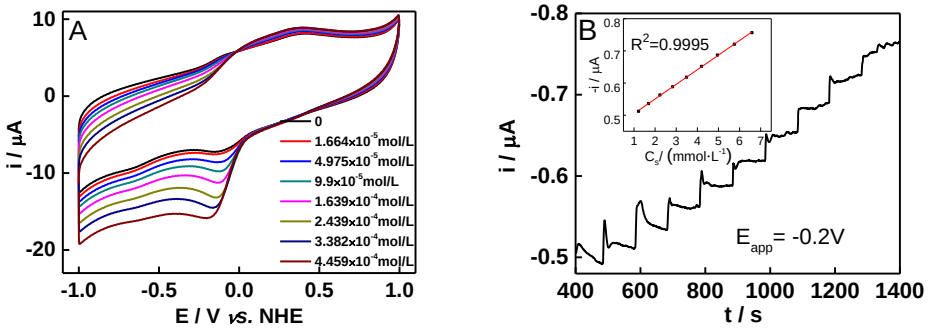

Figure 13. CV curves (A) and CA curve (B) of Hb/H_3IDC-ZnO/GCE in static PBS (pH=7.0) with different contents of hydrogen peroxide, scanning rate of 200 mV•s^{-1} for Fig.13A and applied potential at -200.0 mV for Fig.13B

Table 1. Entry in calculated K_M for Hb based electrodes with different chemical composition and physiochemical feature

Serial number	Material	Structure of electrode	K_M(μM)	References
1	ZnO hollow spheres	Hb/ZHS/Au electrode	500	[31]
2	SWCNT	Hb/SWCNT/CTS/Au electrode	820	[19]
3	PHD/MWCNTs	Hb/PHD/MWCNTs/GCE	510	[46]
4	PANI/SnO_2NF	Hb/PANI/SnO_2NF/CTS/GCE	150	[18]
5	PPy@PSMA-g-4ABS	Hb/PPy@PSMA-g-4ABS/GCE	450	[17]
6	PHB	Hb/PHB/PG	1076	[47]
7	Graphene/CTS	Hb/Graphene/CTS	344	[48]
8	ZnO-H_3IDC*	Hb/H_3IDC-ZnO/CTS/GCE	893	This work

Note: GCE-Glassy carbon electrode; PG-Pyrolytic graphite electrode

3.3 Reproducibility, long-term usability and heat-resistance in Hb-induced electrocatalytic reduction of hydrogen peroxide

The reproducibility, long-term stability, and dependence of the catalytic efficiency on the

operational temperature of the enzyme-induced electrocatalytic reduction of hydrogen peroxide for Hb/H_3IDC-ZnO/GCE are analyzed in Fig.14A, B and C, respectively. Fig.14A shows a minor difference in the catalytic current among the six Hb-based electrodes and RSD was calculated as approximately 4.6%. This suggests an excellent reproducibility of the catalytic function for Hb-based electrodes. Additionally Fig.14B demonstrated that the catalytic performance would attenuate over time due to the decrease in the catalytic activity of Hb incorporation into the complex with time as well as the interference in the catalytic mechanism between anchored Hb and H_3IDC-ZnO composite as discussed earlier. Overall, the residual catalytic current could be retained only by 53.9% of the initial value after storage in the refrigerator for 10 days. This result indicates that the long-term utilization in catalysis of H_2O_2 electrochemical reduction for Hb-based electrode was medium in comparison to other similar systems [49]. Fig.14C implies that the optimal temperature of operation was 339 K and the heat-resistance of immobilized Hb was improved compared with the free Hb. The adjacent coordination described previously could contribute to this advantage and this assumption was supported by the fact that the intensity of fluorescence emission at 360 nm for Hb incorporation into a Chitosan thin film would be reduced to a great extent under the operational temperature of 339 K (data not shown). Furthermore, the attenuation in the catalytic current at higher temperatures could be due to the decomposition of the substrate. This assumption is supported by the fact that a sharp decrease in the catalytic current at temperatures under 362 K is observed, and the remarkable increase in dissolved oxygen concentration in the electrolyte was successfully monitored by a Clark electrode.

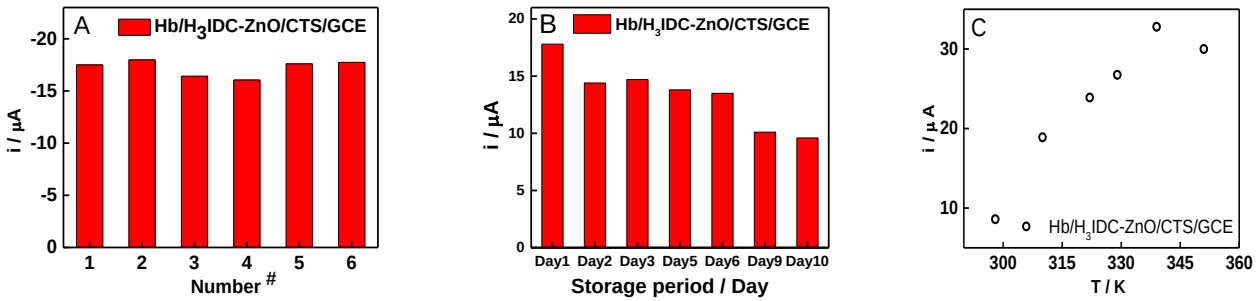

Figure 14. Reproducibility, long-term usability and heat-resistance for electrocatalytic function on electrochemical reduction of H_2O_2 characterized by CV, operational parameters being similar to that presented in Fig.13A, consistency of substrate: 0.25 mM

4. CONCLUSIONS

Petaloid-shaped ZnO surface-tailored by the derivative of imidazole could accommodate Hb molecules through the synergistic effect of covalent coupling and adjacent coordination. The impact of the interaction between components of the complex and Hb anchoring on the structural parameters and physio-chemical features of Hb integration were investigated by a variety of experimental

techniques. Results from experiments can be generalized as follows:

1) Complicated interactions between H_3IDC and immobilized Hb resulted in the apparent variation of the chemical feature of the composite surface after Hb integration, which improved its hydrophilicity and heat-resistance. These interactions would not impose great influence on the inherent configuration of Hb integration into the ZnO-H_3IDC composite. Inherent catalytic activity to the substrate of Hb could be preserved to a considerable degree in spite of considerable hindrance in substrate binding.

2) The combination of Hb with H_3IDC would lead to the formation of a complex without fluorescence emission and could alter the route of charge conveyance between the cofactors in Hb and the conductive interface. Electrochemical reactions of Hb-based electrode featured with a unique mixed mode of surface-controlled reaction from cofactors of Hb coupling to composite and swinging from electro-active groups in composite. Electrochemical reactions of the heme sites in Hb could be attributed to a typical redox process with one proton and two electrons involved. The process of substrate diffusion from the bulk solution to the surface of the electrode was determined as the rate determining step of the whole catalysis.

ACKNOWLEDGEMENTS

The research presented in this submission was subsidized by the National Natural Science Foundation of China (No. 31560249) and the “13th five-year” plan for key discipline chemistry, Xinjiang normal university.

References

1. P. N. Asrami, S. A. Mozaffari, M. S. Tehrani and P. A. Azar, *Int. J. Biol. Macromol*., 118(2018) 649.
2. N. Muthuchamy, R. Atchudan, T. N. J. I. Edison, S. Perumal and Y. R. Lee, *J. Electroanal. Chem*., 816(2018) 195.
3. F. Zhou, W. Jing, Y. Xu, Z. Chen, Z. Jiang and Z. Wei, *Sensor. Actuat B-Chem*., 284(2019) 377.
4. A. K. M. Kafi, S. Alim, R. Jose and M. M. Yusoff, *J. Electroanal. Chem*., 852(2019) 113550.
5. A. Brune, G. Jeong, P. A. Liddell, T. Sotomura, T. A. Moore, A. L. Moore and D. Gust, *Langmuir*., 20(2004) 8366.
6. W. Zhao, X. Li, Z. Wen, X. Niu, Q. Shen, Z. Sun and R. Dong, *Int. J. Electrochem. Sci*., 12(2017) 4025.
7. H. Zeng, S. Zhao, L. Gong and Z. Su, *Chin. J. Appl. Chem*., 30(2013) 436.
8. M. M. Barsan, V. Pifferi, L. Falciola and C. M. Brett, *Anal. Chim. Acta*, 927(2016) 35.
9. B. Fang, C. Zhang, G. Wang, M. Wang and Y. Ji, *Sensor. Actuat. B-Chem*., 155(2011) 304.
10. Y. Zhao, W. Li, L. Pan, D. Zhai, Y. Wang, L. Li, W. Cheng, W. Yin, X. Wang, J. B. Xu and Y. Shi, *Sci. Rep*., 6(2016) 32327.
11. X. Fang, J. Liu, J. Wang, H. Zhao, H. Ren and Z. Li, *Biosens. Bioelectron*., 97(2017) 218.
12. D. Yuan, Q. Zhang, Z. Hou, D. Li, J. Zhang and H. Zhang, *Mater. Rep*., 20(2006) 69.
13. Y. Yang, H. Zeng, W. S. Huo and Y. H. Zhang, *J. Inorg. Organomet. Polym*., 27(2017) 201.
14. H. Wen, X. Gong, Z. Jia, P. Han, B. Lin, S. Ye, Y. Sun, X. Zhang and H. Yang, *Dyes. Pigments*., 130(2016) 16.
15. H. Wen, X. Gong, P. Han, B. Lin, L. Zhang, S. Ye, Y. Sun, X. Zhang and H. Yang, *RSC. Adv*., 6(2016) 69277.
16. T. M. Ma, H. Zeng, S. X. Zhao and W. S. Huo, *J. Inorg. Organomet. Polym*., 29(2019) 279.

17. M. Baghayeri, E. N. Zare and M. M. Lakouraj, *Microchim. Acta*, 182(2015) 771.
18. A. K. M. Kafi, Q. Wali, R. Jose, T. K. Biswas and M. M. Yusoff, *Microchim. Acta*, 184(2017) 4443.
19. A. K. M. Kafi, C. C. L. Yam, N. S. Azmi and M. M. Yusoff, *J. Nanosci. Nanotechno*., 18(2018) 2422.
20. H. Zeng, W. S. Huo, F. Wang and T. M. Ma, *Macromol. Res*., 27(2019) 963.
21. S. Z. Yang and L. Y. Yu, *Anhui. Chem. Ind*., 44(2018) 40.
22. H. Toiserkani, *Polym. Advan. Technol*., 29(2018) 1834.
23. H. Y. Zhao, H. M. Zhou, J. X. Zhang, W. Zheng and Y. F. Zheng, *Biosens. Bioelectron*., 25(2009) 463.
24. J. Qiu, H. Peng and R. Liang, *Electrochem. Commun*., 9(2007) 2734.
25. P. Ma, J. Tan, H. Cheng Y. Fang, Y. Wang, Y. Dai, S. Fang, X. Zhou and Y. Lin, *Appl. Surf. Sci*., 427(2018) 458.
26. M. Zhang, Y. H. Zhang, T. M. Ma and H. Zeng, *Chem. Phys. Lett*., 738(2020) 136904.
27. J. Zhang, R. Zhang, L. H. Zhao and S. Q. Sun, *CrystEngComm*., 14(2012) 613.
28. L. Zhao, H. Zhang, J. Zhang, W. Zong and R. Liu, *Luminescence*, 34(2019) 290.
29. C. X. Tan and T. Xiao, *J. Northwest. Normal. Univ*., 41(2005) 94.
30. W. Chen, X. Niu, X. Li, X. Li, G. Li, B. He, Q. Li and W. Sun, *Mat. Sci. Eng. C-Mater.*, 80(2017) 135.
31. C. Liu, J. Xu and Z. Wu, *Bioproce. Biosyst. Eng*., 34(2011) 931.
32. L. Yao, Y. Xi, G. Xi and Y. Feng, *J. Alloy. Compd.*, 680(2016) 73.
33. L. Shuai, Z. Chen, K. Y. Wang and Q. Wang, *Pharm. Biotechnol*., 22(2015) 53.
34. R. Wang, Y. Yin, R. Wang, Y. Xie, B. Ge, Z. Li, Z. Li, J. Shi and J. Chang, *J. Lumin*., 144 (2013) 79.
35. J. Liu, X. Gong, L. Xu, L. Zhang and P. Gong, *J. Instrumental. Anal*., 37(2018) 389.
36. H. Mao, B. F. Cai, B. Zhao and Z. W. Wang, *Chin. J. Appl. Chem*., 26 (2009) 1332.
37. Y. Liu, M. Wang, F. Zhao, Z. Xu and S. J. Dong, *Biosens. Bioelectron*., 21(2005) 984.
38. H. Zheng, J. B. Hu and Q. L. Li, *Acta. Chim. Sinica*, 64(2006) 806.
39. W. E. Farneth, B. A. Diner, T. D. Gierke and M. B. D′Amore, *J. Electroanal. Chem*., 581(2005) 190.
40. W. Zheng, Study on the Structure and Electrochemical Properties of Carbon nanotube biological interface, Harbin Engineering University, china, 2006, 36.
41. W. Ma and D. Tian, *Bioelectrochemistry*, 78(2010) 106.
42. L. Zhang, Q. Zhang, X. Lu and J. Li, *Biosens. Bioelectron*., 23(2007) 102.
43. Y. Liu, X. Qu, H. Guo, H. Chen, B. Liu and S. Dong, *Biosens. Bioelectron*., 21(2006) 2195.
44. I. Willner, V. Heleg-Shabtai, R. Blonder, E. Katz and G. Tao, *J. Am. Chem. Soc*., 118 (1996) 10321.
45. G.C. Zhang, Hydrogen peroxide production technology, Chemical Industry press, (2012) China.
46. Z. Wang, J. Yi and S. Yang, *Sensor. Actuat. B-Chem*., 176 (2013) 211.
47. X. Ma, X. Liu, H. Xiao and G. Li, *Biosens. Bioelectron*., 20(2005) 1836.
48. H. Xu, H. Dai and G. Chen, *Talanta*, 81(2010) 334.
49. T. Zhan, X. Wang, Y. Zhang, Y. Song, X. Liu, J. Xu and W. Hou, *Sensor. Actuat. B-Chem*., 220 (2015) 1232.

© 2020 The Authors. Published by ESG (www.electrochemsci.org). This article is an open access article distributed under the terms and conditions of the Creative Commons Attribution license (http://creativecommons.org/licenses/by/4.0/).